STUDIA UBB CHEMIA, LXX, 3, 2025 (p. 55-64)
(RECOMMENDED CITATION)
DOI:10.24193/subbchem.2025.3.04

SALT TEMPLATE-ASSISTED SYNTHESIS OF β-CYCLODEXTRIN DERIVED 3D CARBON NANOCORALS

Jinyan HUANG[a], Ye XING[b], Haichao LI[b,c,*]

ABSTRACT. Carbon nanomaterials have great scientific importance due to their unique physicochemical properties. They show great promise in the fields of catalysis, energy storage and environmental treatment. However, the traditional synthesis methods are characterized by cumbersome steps, difficult template removal and high environmental costs. In this study, a salt template-assisted strategy was innovatively employed with β-cyclodextrin (β-CD) as a renewable carbon source and NaCl as a dynamic separation template. Controlled preparation of 3D carbon nanocorals (CNCs) has been achieved for the first time by regulating the self-assembly and carbonization process. XRD and Raman spectroscopy showed that the graphite microcrystalline ordering of the material increased significantly with increasing concentration, and the graphite layer spacing was reduced from 0.453 nm to 0.443 nm. In addition, the NaCl template has a recovery rate of over 90% after washing. Meanwhile the sodium chloride can be reused after recycling. It is in line with the concept of green chemistry. This strategy provides a new idea for the precise construction of complex carbon nanostructures.

Keywords: *3D Carbon Nanocorals, Salt Template-assisted, β-Cyclodextrin, Carbon nanomaterial.*

[a] *Qinghai Institute for Advanced Study, Qinghai University, Xining, 810016, Qinghai, China.*
[b] *School of Chemistry and Materials Science, Qinghai Minzu University, Xining, 810007, Qinghai, China.*
[c] *Qinghai Institute for Advanced Study, Qinghai Minzu University, Xining, 810007, Qinghai, China.*
[*] *Corresponding author: lihaichao@vip.163.com*

INTRODUCTION

Carbon nanomaterials, due to their unique physicochemical properties, show broad application prospects in the fields of catalysis, energy storage, biomedical and environmental treatment [1-3]. In recent years, researchers have devoted themselves to the development of structurally novel carbon nanomaterials to break through the limitations of conventional materials in terms of specific surface area, mass transfer efficiency and stability. The 3D porous carbon materials have become a research hotspot due to their high specific surface area, rich pore structure and excellent electron transport properties [4]. However, the existing synthesis methods such as hard template method and hydrothermal method still face the problems of cumbersome steps, difficult template removal, high cost and environmental burden [5,6]. The traditional hard template method requires the use of corrosive reagent HF to remove silica templates, which is not only dangerous to operate, but also limits the large-scale production of the material [7]. Therefore, the development of green, efficient and structurally controllable synthesis strategies has become an important challenge in the field of carbon nanomaterials.

In recent years, the salt template method has attracted much attention due to its advantages such as environmental friendliness, easy operation and template recyclability [8,9]. Literature data reveals that salt lakes represents special environmental systems proving the green approach of the chosen method [10]. Du et al. successfully prepared size-tunable carbon nanoframes using the DTAB @ NaCl self-assembly strategy and achieved precise control of the structure by modulating the surfactant concentration [11]. Lin et al. further extended the method by synthesizing carbon nanoframes and hollow carbon nanocubes using the SB3-12 @ NaCl system, revealing the key role of salt templates in morphology modulation [12]. These studies provide an important reference for the application of the salt template method in the design of carbon nanostructures. However, the existing results are still limited to simple geometric forms such as frames or hollow spheres. There is no breakthrough yet in constructing complex 3D network structures.

Cyclodextrins as a renewable biomass carbon source, show unique potential in nanomaterial synthesis due to their unique ring-like cavity structure and tunable self-assembly properties [13]. Xing et al. developed hollow carbon nanospheres based on a salt separation strategy of α-cyclodextrin and NaCl, with a shell thickness that can be flexibly adjusted by the precursor concentration [14]. Compared to α-cyclodextrin, β-cyclodextrin has a larger cavity size and stronger hydrophobic interactions, making it easier

to form multilayered supramolecular assemblies. By modulating the cyclodextrin concentration, the aggregates may take the shape of rods, disks, oblong spheres, globules, bilayers, vesicles, or reversible micelles [15]. However, the aggregation of cyclodextrins in NaCl solution has been rarely reported.

In this study, a salt template-assisted strategy using β-cyclodextrin as a carbon source and NaCl as a dynamic template is reported. We demonstrate that β-cyclodextrin can form 3D carbon nanocoral structures under NaCl assistance, with the template recovered by water washing for green chemistry compliance. This work provides a new approach for controllable synthesis of complex carbon nanostructures and expands the application of cyclodextrin-based functional materials.

RESULTS AND DISCUSSION

The 3D CNCs prepared at different concentrations have similar morphology. For example, Figure 1 shows SEM images of CNCs prepared at 10 mM at different magnifications. The formation of carbon nanocorals (CNCs) from β-CD assisted by NaCl template is mainly due to the self-assembly property of β-CD and the dynamic domain-limiting effect of NaCl template. β-CD has a unique cyclic cavity structure and a tunable self-assembly ability. β-CD molecules spontaneously form dispersed, small-sized aggregates through hydrogen bonding and hydrophobic interactions. This self-assembly behavior was further modulated in NaCl solution. The addition of NaCl enhanced the intermolecular interactions between β-CD molecules, possibly through an electrostatic shielding effect or by changing the solvent polarity, thus promoting the formation of coral-like structures. NaCl provides a dynamic template during high-temperature carbonization. Through the domain-limiting effect of its crystal structure, it guides the formation of specific 3D network structures of β-CD derived carbon precursors during pyrolysis. The facile nature of NaCl in water allows the final product to retain the coral-like morphology formed by the template [16]. The formation of coral-like structures by β-CD assisted by the NaCl template is the result of a combination of self-assembly behavior, dynamic template domain-limiting effects, and concentration-dependent interactions. This strategy provides a new idea for the controlled synthesis of complex 3D carbon nanostructures.

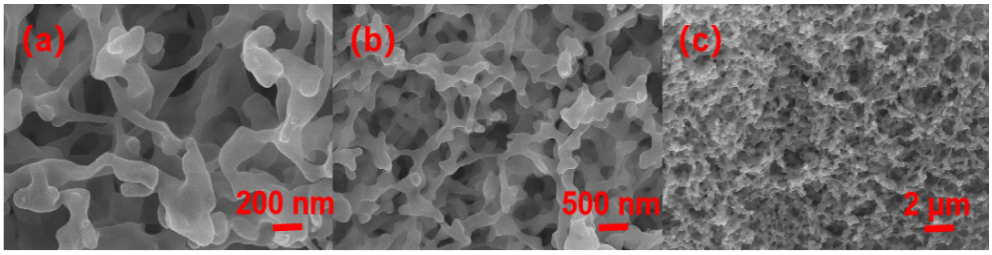

Figure 1. SEM images of CNCs at different magnifications

The degree of graphitization reflects the degree of ordering of carbon atoms to form hexagonal graphite crystals and is an important indicator of the quality of graphite materials. The degree of graphitization of the synthesized CNCs at concentrations of 5 mM, 10 mM and 20 mM increased significantly with increasing concentration as detected by XRD. As shown in Figure 2, the structures were analyzed by XRD, and all samples with (002) crystalline facets at 2θ = 26° had characteristic diffraction curves of carbon, with no crystallographic Bragg peaks detected, which is characteristic of amorphous structures [17, 18]. As the concentration increases, the (002) peak at 2θ ≈ 26.5° (assigned to hexagonal graphite, PDF#41-1487) becomes sharper and more intense, indicating microcrystalline growth. This assignment is validated by matching the peak position to the standard graphite phase (a=2.461 Å, c=6.708 Å, ICDD PDF#41-1487). The peak shift to higher Bragg angles (evident in Figure XRD) corresponds to a decrease in d_{002} spacing from 0.453 nm (5 mM) to 0.443 nm (20 mM) as calculated by Bragg's law (Table 1). This narrowing of interlayer spacing aligns with the increased peak intensity, both indicators of improved graphitic ordering. While the 20 mM sample shows a d_{002} value (0.443 nm) slightly larger than fully graphitized carbon (0.335 nm), the trend confirms enhanced local crystallinity with concentration [19]. The apparent (104) crystal surfaces in the Figure 2 are from $CaCO_3$ and $CaMg(CO_3)_2$, and since Ca and Mg are not added to the raw materials, it is hypothesized that they may be due to the abundance of minerals in the tap water in the Qinghai region. Indeed the natural water can contain significant amounts of $CaCO_3$ crystallized as calcite and micro dispersoids of $CaMg(CO_3)_2$ crystallized as dolomite occurring form the shore rocks, but dissolved Ca^{2+} and Mg^{2+} ions re-crystallizes as pseudo-dolomite. The diffraction peak in Figure 2 at about 29.3° belongs to calcite and the peak of about 30.98° belongs to dolomite [20, 21]. At the same time the work of the ultrapure water machine at high altitude is affected, resulting in some of the ions not being removed cleanly.

Table 1. XRD parameters of 5 mM, 10 mM and 20 mM

	5 mM	**10 mM**	**20 mM**
$2\theta_{(002)}$/(°)	19.58	19.90	20.02
d_{002}/nm	0.453	0.445	0.443

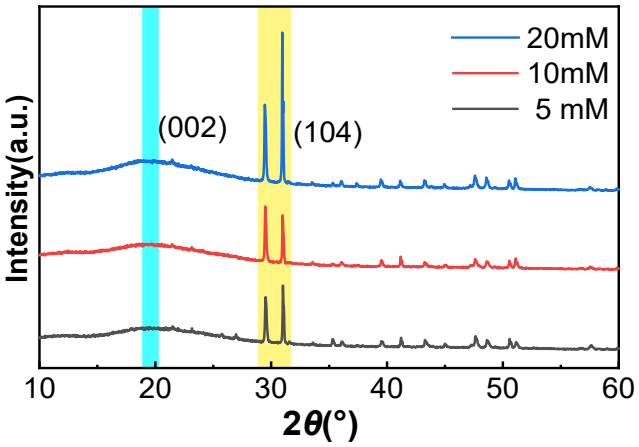

Figure 2. XRD patterns of CNCs at different concentrations

Raman spectroscopy can provide information about the graphite crystal structure and structural defects in graphite, and the data can be used to complement XRD data. As shown in Figure 3, at concentrations of 5 mM, 10 mM and 20 mM, D bond, G bond and D+G bond appeared simultaneously in the samples, which is a typical feature of amorphous carbon. The intensity ratio of the D and G bonds (I_D/I_G) is another key parameter to analyze the degree of graphitization [22]. The intensity ratios of carbon nanomaterials (I_D/I_G) were 0.931, 0.862 and 0.736 at concentrations of 5 mM, 10 mM and 20 mM. The height difference between the D and G bonds decreased significantly with increasing concentration. This suggests a gradual reduction of microcrystalline defects within the CNCs as they transform from a graphite disordered layer structure to an ordered structure [23]. The broad and weak D+G bonds near 2700 cm^{-1} also indicate again that there are some defects in the prepared CNCs graphite layer structure. Raman spectroscopy again verifies that the concentration increase can effectively induce the evolution of carbon nanomaterials towards ordered structures.

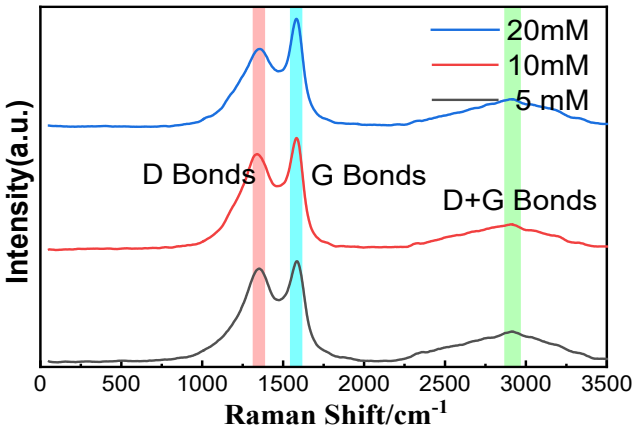

Figure 3. Raman spectra of CNCs at different concentrations

The elemental test composition of carbon nanomaterial XPS is shown in Table 2. There is no significant change in the elemental content, which is mainly composed of C and O elements, and most of them are carbon elements. As the β-CD concentration increased to 10 mM, the carbon content of CNCs reached its maximum. The carbon content of CNCs decreased when the β-CD concentration increased to 20 mM. Due to the change in concentration that the structure of β-CD aggregates changed, which is beneficial to the overflow of small molecule hydrocarbons during thermolysis. XPS is commonly used to characterize the chemical structure of material surfaces. Figure 4 show the full XPS spectra of the different samples, verifying that the main components of the prepared CNCs are the elements C and O. Figures (5, 6, 7) show the split peaks of C1s and O1s, with the C1s spectrum splitting into three peaks. The results show that in combination with elemental analysis, there are three possible bonding forms of C, C=C (284.8 eV), C-O (286.4 eV) and C-O (288.4 eV). O1s splits into 2 peaks, C-O (530.8 eV) and C=O (529.5 eV). XPS data showed that the prepared CNCs were all amorphous carbon with similar surface chemical structure [17].

Table 2. Elemental analysis of CNCs at different concentrations

Sample	C (at.%)	O (at.%)
5 mM	72.26	26.28
10 mM	87.14	12.15
20 mM	85.04	14.33

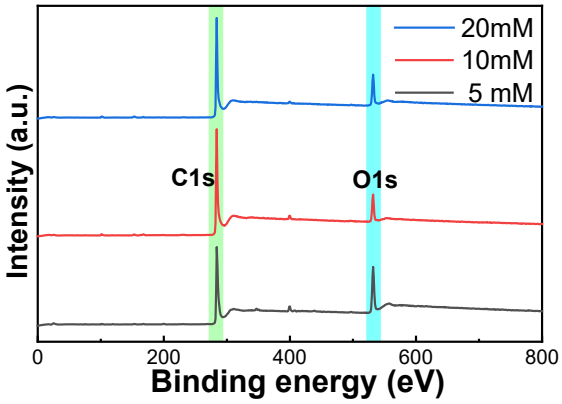

Figure 4. Full XPS spectra of CNCs at different concentrations

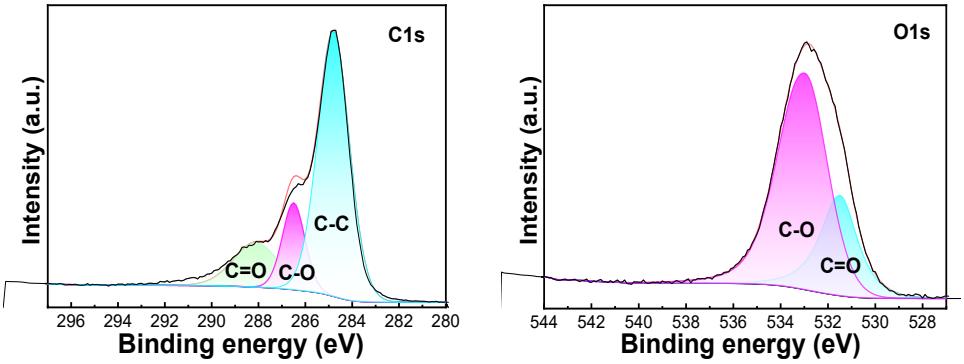

Figure 5. C1s and O1s XPS spectra of CNCs at 5 mM

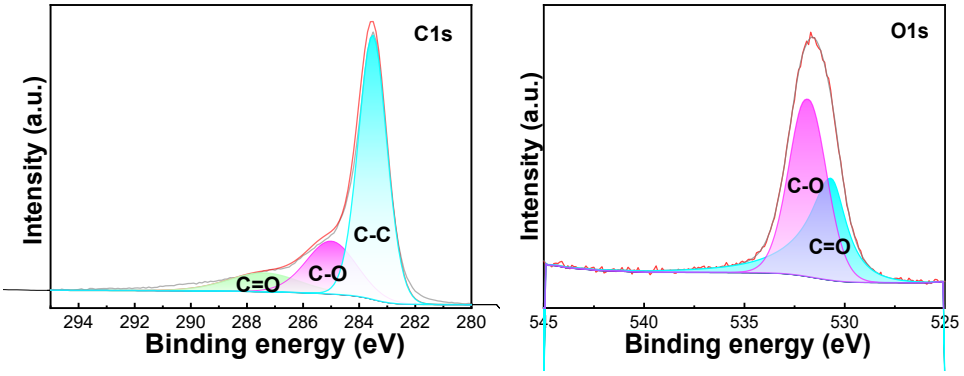

Figure 6. C1s and O1s XPS spectra of CNCs at 10 mM

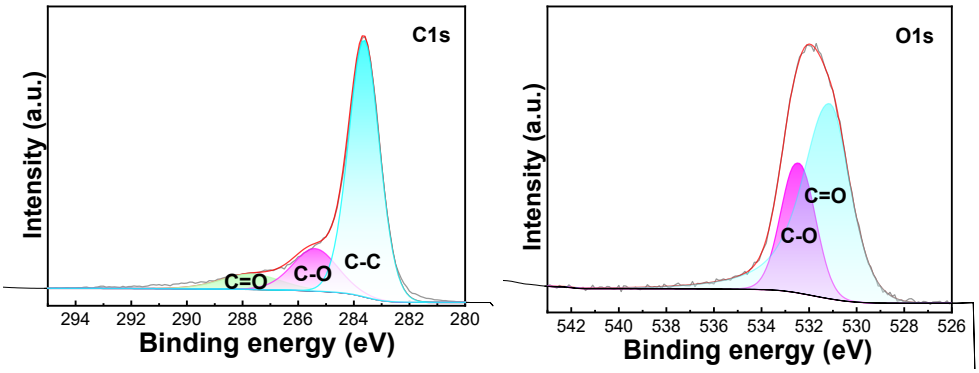

Figure 7. XPS spectra of C1s and O1s of CNCs at 20 mM

CONCLUSIONS

In this study, a novel synthesis method of 3D carbon nanocorals (CNCs) based on a salt template-assisted strategy was successfully developed. By using β-Cyclodextrin (β-CD), a renewable carbon source, combined with the domain-limiting effect of NaCl dynamic templates. Controllable preparation of coral-like carbon 3D networks was realized for the first time. The unique self-assembly behavior of β-CD, driven by hydrogen bonding and hydrophobic interactions, combined with the dynamic domain-limiting effect of NaCl, enabled the formation of well-defined 3D coral-like carbon nanostructures. The NaCl template not only guided the morphology but also facilitated the creation of network. The method efficiently recovers NaCl templates by water washing, avoiding the dependence on corrosive reagents such as HF in the traditional hard template method. This is in line with the concept of green chemistry. This study not only provides new ideas for the controllable synthesis of complex carbon nanostructures, but also expands the boundary for the application of cyclodextrin-based functional materials in energy and environmental fields.

EXPERIMENTAL SECTION

β-Cyclodextrin (β-CD) and NaCl, all the chemicals used were analytically pure reagents purchased from Aladdin Biochemical Technology Co., Ltd. in Shanghai, China, and the water used in the experiments was ultrapure water.

Solutions of β-CD at 5 mM, 10 mM and 20 mM were prepared in a crucible and allowed to stand for 48 hours to fully form the aggregates. The aggregates of β-CD were segregated by adding an appropriate amount of salt to the crucible

and the mixture was referred to as the β-CD @ NaCl system. The prepared β-CD @ NaCl system was carbonized in a muffle furnace. The temperature was increased to 700°C at a rate of 5°C/min. Samples were left at the highest temperature for 2 h to ensure complete carbonization. At the end of the carbonization process, wait for natural cooling to room temperature, remove the samples, and place the carbonization products extracted from the muffle furnace in a 1000 mL beaker with excess boiling water. After complete dissolution in NaCl, the target product, carbon nanocorals (CNCs), was obtained by filtration through a 200 nm microporous filtration membrane. After rough calculations, the NaCl recovery reached more than 90%.

The morphology of CNHCs was observed by SEM (ZEISS GeminiSEM 500, Germany). The crystalline structure parameters of the samples were determined using a D/MAX-B type X-ray diffractometer from RIKEN, Japan. Cu target radiation (λ = 0.154056 nm) and scanned the sample at a scanning speed of 4° min^{-1} in the range of 2θ=10°-80°. Surface functional groups were analysed by X-ray photoelectron spectroscopy with the ESCALAB 250XI model from Thermo Fisher Scientific, USA. Each photoelectron spectral region was scanned several times to obtain a good signal ratio. The C1s peak was set to 284.6 eV and used as an internal standard for the other peaks.

ACKNOWLEDGMENTS

This work was supported by the Key R&D and Transformation Program of Qinghai (2022-QY-210), and Research Teams of Kunlun Scholars Project of Qinghai Province.

REFERENCES

1. Q. Xu; H. Cai; W. Li; M. Wu; Y. Wu; X. Gong; *J. Mater. Chem. A,* **2022**, 10, 14709-14731.
2. D. G. Saini; J. Kaushik; R. Aggarwal; K.M. Tripathi; S.K. Sonkar; *ACS Appl. Nano Mater.,* **2021**, 4, 12825-12844.
3. Y. Yin; X. Hou; B. Wu; J. Dong; M. Yao; *Adv. Funct. Mater.,* **2024**, 34, 2411472.
4. C. Jiang; H. Liu; J. Ye; N. Wang; Y. Tang; C. He; H. Zhang; B. Chen; *Batteries & Supercaps,* **2025**, 8, e202400563.
5. V. Malgras; J. Tang; J. Wang; J. Kim; N.L. Torad; S. Dutta; K. Ariga; M.S.A. Hossain; Y. Yamauchi; K.C. Wu; *J Nanosci. Nanotechno.,* **2019**, 19, 3673-3685.
6. H. Liang; R. Sun; B. Song; Q. Sun; P. Peng; D. She; *J. Hazard. Mater.,* **2020**, 387, 121987.

7. Y. Chen; L. Tong; G. Lin; W. Zhang; Q. Zeng; X. Liu; *J. Mater. Sci-Mater.* El., **2021**, 32, 2774-2783.
8. Q. Chen; H. Li; *Nanomaterials*, **2022**, 12, 1652.
9. X. Kang; H. Li; X. Yang; Z. Lin; *RSC Adv.*, **2024**, 14, 28215-28223.
10. L., Rus; S.E. Avram; V Micle, Romania. *Studia UBB Chemia,* **2020**, 65, 257–268.
11. B. Du; H. Li; C. Zhang; Q. Ji; Adv. Mater. Int., **2024**, 11, 2300832.
12. Z. Lin; B. Du; C. Zhang; Q. Ji; X. Yang; H. Li; *Adv. Mater. Int.*, **2024**, 11, 2400509.
13. A. Ryzhakov; T. Do Thi; J. Stappaerts; L. Bertoletti; K. Kimpe; A.R.S. Couto; P. Saokham; V. Mooter; G., Augustijns; P. Somsen; *J. Phar. Sci.,* **2016**, 105, 2556-2569.
14. Y. Xing; Y.N. Wang; H. Li; *Fuller Nanotub. Car. N.,* **2024**, 32, 1135-1139.
15. D. Duchene; A. Bochot; *Int J Pharmaceut.*, **2016**, 514, 58-72.
16. S. Hao; Q. Zhang; Y. Shi; Q. Guo; P. Li; J. Huang; *Biomass. Convers. Bior.,* **2024**, 14, 9581-9594.
17. Y. Guangzhi; Y. Binbin; S. Shen; T. Zhihong; Y. Dengguang; Y. Junhe; *RSC Adv.,* **2017**, 7, 16341-16347.
18. J. Tu; H. Li; J. Zou; S. Zeng; Q. Zhang; L. Yu; X. Zeng; *Dalton T.*, **2018**, 47, 16909-16917.
19. H. Wei; W. Liu; T. Liu; Q. Li; H. Li; *Mater. Res. Express,* **2019**, 6, 0950b8.
20. A. Tamas; L. Cocheci; L. Lupa; *Studia UBB Chemia,* **2025**, 70, 147–158.
21. S.E. Avram; D.V. Platon; L.B. Tudoran; G. Borodi; I. Petean; *Appl. Sci.,* **2024**, 14,10806.
22. Y. Gong; L. Xie; H. Li; Y. Wang; *Chem. Commun*., **2014**, 50, 12633-12636.
23. H. Nishihara; T. Kyotani; *Adv. Mater.,* **2012**, 24, 4473-4498.